Journal of Magnetism and Magnetic Materials 475 (2019) 703–714

Contents lists available at ScienceDirect

Journal of Magnetism and Magnetic Materials

journal homepage: www.elsevier.com/locate/jmmm

Research articles

Experimental and numerical analysis of the magnetophoresis of magnetic nanoparticles under the influence of cylindrical permanent magnet

Jiajia Sun, Zongqian Shi*, Shuang Chen, Shenli Jia

State Key Laboratory of Electrical Insulation and Power Equipment, Xi'an Jiaotong University, No. 28 Xianning West Road, Xi'an, Shaanxi Province 710049, China

ARTICLE INFO

Keywords:
Magnetic nanoparticles
Magnetophoresis
Coupled particle-fluid method
Dye-tracing experiment

ABSTRACT

Dye-tracing and concentration-measuring experiments are carried out to investigate the magnetophoresis of magnetic nanoparticles (MNP) in the presence of an external cylindrical permanent magnet. The magnetophoresis of MNP, inducing an obvious forced-convective flowing of the carrier fluid, which can be observed by visualizing flowing of carrier fluid, results in a temporal and spatial variation of particle concentration. Moreover, in order to get insight into the physical mechanisms of magnetophoresis of MNP, a coupled particle-fluid analysis, in which the non-linear drift-diffusion differential equation is incorporated into the Navier-Stokes equation, is adopted to discuss the influence of particle-fluid interaction on the variation of particle concentration and the kinetics of carrier fluid. It is worth noting that the equivalent current source (ECS) method is adopted to obtain a closed-form field analysis, which provides exactly prediction of the Kelvin force and enables magnetophoretic analysis more efficient. In dye-tracing experiments, an obvious vortex can be observed as the methylene blue moves with the convection of carrier fluid. Furthermore, this phenomenon is also predicted by using the coupled particle-fluid model. A comparison between the experimental and numerical results shows that the hydrodynamic interactions between MNP and carrier fluid plays an important role in inducing forced-convective flowing of carrier fluid and enhancing the magnetophoresis of MNP. Furthermore, these results also denote that the coupled particle-fluid model provides a more efficient and accurate method in investigating the magnetophoresis of MNP.

1. Introduction

Due to the unique magnetic property, magnetic nanoparticles have a corresponding proliferation of applications in various fields including magnetofection, drug delivery, micro-mixing, bioseparation, bio-chemical sensing, and thermal systems [1–8]. More generally, there are ongoing emphasis on the fabrication of functional magnetic nanoparticles, which can be encapsulated with biomolecule, such as gene, medicine, proteins, and whole cell etc. [1,3,5,9]. Bounded with a target biomaterial, the magnetic nanoparticles can be separated from carrier fluid or immobilized at special tissues when they are subjected to an external gradient magnetic field. For implementing such functionalities, it is necessary to carry out experimental and numerical investigation on the magnetophoresis of MNP, which is defined as manipulation of MNP in a viscous medium by using gradient magnetic field.

The behavior of MNP, suspended in a carrier fluid, is related to many factors, involving Kelvin force, viscous force, magnetic dipole-dipole interaction, electric double-layer interactions, surfactant force, and van der Waals force [10]. Taking all of the forces into consideration is complicated and increases the difficulty of computation. Thus, different models are adopted to simplify the analysis. For a dilute MNP suspension liquid (particle concentration $c << 1$), the interactions between the particles are negligible, and the Lagrangian or the Eulerian methods are used to predict the MNP transport [1]. In the Lagrangian approach, the nanoparticles are regarded as discrete phase, and the trajectory of each particle is obtained by integrating the Newtonian law. Besides, this approach is appropriate when the Brownian motion is negligible [11]. In the Eulerian approach, the drift-diffusion equation is adopted to model the behavior of the particles by using the time-dependent particle concentration, in which the magnetic force-induced drift and the Brownian diffusion are taken into consideration [12]. Gerber et al. used a criterion ($|\boldsymbol{F}|D_p \leq kT$) to estimate the significance of Brownian motion [13]. The $|\boldsymbol{F}|$ is the magnitude of total force acting on a particle, D_p is the diameter of particle, k is the Boltzmann constant, and T is the absolute temperature. For particles with size smaller than the critical particle diameter $D_{c,p}$ ($=kT/|\boldsymbol{F}|$), the Brownian motion of the particles should not be ignored. It should be noted that the motion of nanoparticles in the presence of magnetic field has a significant

* Corresponding author.
E-mail address: zqshi@mail.xjtu.edu.cn (Z. Shi).

https://doi.org/10.1016/j.jmmm.2018.11.124
Received 17 May 2018; Received in revised form 28 November 2018; Accepted 28 November 2018
Available online 05 December 2018
0304-8853/

impact on the behavior of the carrier fluid as well. To emphasize this point, the Navier-Strokes equations are also adopted to take the particle-induced flow into account.

By coupling Navier-Strokes equation with drift-diffusion equation, Cao used a finite element method to investigate the variation of the particle concentration in 2D microchannel under different permanent magnets [14], whose magnetic field is numerically calculated by finite element method. Besides, for the particles with dimension above $D_{c,p}$, the effect of the particles-induced flow on the trajectory of each nanoparticle in 2D microchannel has also been investigated by using the Lagrangian method coupled with Navier-Strokes equation[15], in which the magnetic field of the rectangle permanent magnet is calculated by using equivalent charge method.

Compared with the simulation, experiment is a more direct method. In the investigation of Teste *et al.*, the number of captured particles was calculated by some parameters and fluorescence signal [16]. In their experiments, the particles were labeled with fluorescence and the fluorescence signal was detected by optical equipment. Schaller *et al.* observed the magnetophoresis of particles via optical microscope and found that the particles could form magnetic chains in this process [17]. Besides, the concentration of particles was measured by optical method for quantifying the particle separation process. In the research of Mykhaylyk O et al., the magnetophoretic velocity of magnetic nanoparticles was characterized by measuring space- and time-resolved extinction profiles using a gravity sedimentation analyser LUMiReader equipped with a set of permanent magnets [18].

Leong *et al.* used the Eulerian model to investigate the distribution of the particle concentration in the presence of a cylindrical permanent magnet, whose magnetic field is described only by *z* component [19]. Besides, they also used the coupled model to verify the influence of the interaction between the particles and carrier fluid by comparing with the experimental results, in which the motion of fluid could be observed by using dye-tracing and concentration-measuring experiments [19]. Moreover, in their latest research [20], the influence of different physical factors, such as particles size, gradient of magnetic field, geometry of cuvette and etc., on the kinetics of magnetic separation was also investigated.

In this study, the magnetophoresis of the magnetic nanoparticles in a standard cuvette is analyzed by using coupled particle-fluid model, dye-tracing and concentration-measuring experiments. By incorporating drift-diffusion equation into Navier-Strokes equation, the influence of interaction between magnetic nanoparticles and carrier fluids on the behavior of magnetic nanoparticles and the kinetics of carrier fluid is discussed. Furthermore, the results of the coupled model are also compared with that of only drift-diffusion equation in order to verify the significance of particle-fluid hydrodynamic interaction. In the dye-tracing experiment, the flowing of carrier fluid is visualized by recording the motion of methylene blue from two views during the magnetophoresis of MNPs. Besides, UV–vis spectrophotometer is adopted to measure the variation of MNP concentration at different locations of MNPs solution. Finally, the radial distribution of magnetic force is also taken into account to illustrate the distribution of captured particles.

2. Experimental configuration

The schematic diagram of the experimental setup is shown in Fig. 1. A standard 1 × 1 × 4 cm cuvette is placed on the top surface of a cylindrical permanent magnet, whose material is neodymium-iron-boron (NdFeB) with radius $R = 6$ mm, height $H = 8$ mm and magnetization $M = 9.55 \times 10^5$ Am^{-1}. A suspension of non-coated magnetite (Fe_3O_4, $\rho_p = 5000\, kg{\cdot}m^{-3}$) spherical nanoparticles in water solution is used in our study, which was provided by Xi'an Ruixi Biological Technology Co., Ltd. The radius of MNP is 25 nm and its saturation magnetization is $M_{sp} = 4.78 \times 10^5$ Am^{-1}. The origin of the Cartesian coordinate locates at the center of top surface of magnet. *S* is the thickness of cuvette

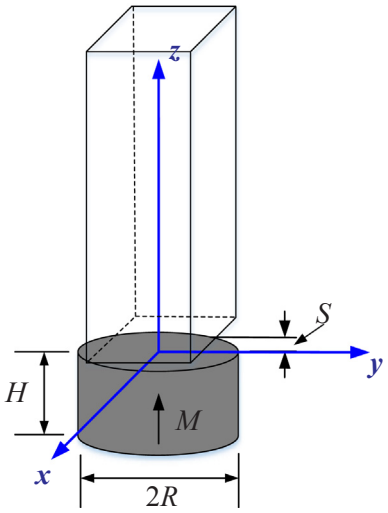

Fig. 1. The schematic diagram of experiment setup.

($S = 1.3$ mm).

2.1. Dye-tracing experiment

At first, 3 mL magnetic nanoparticle suspension is injected into a cuvette. Then, in order to observe the kinetics of carrier fluid, 40 μL methylene blue (MB) solution with a concentration of 3000 mg/L is injected carefully to the bottom of the cuvette. Even though the negative zeta potential magnetic nanoparticles will be covered by positively charged dye molecules, excess injection of MB ensures abundant of freely suspended MB that can be used to trace the flowing of carrier fluid [19]. After injecting of MB, the cuvette is moved onto the top surface of cylindrical permanent magnet. At the same time, a camera is used to record the motion of carrier fluid from front view as shown in Fig. 2(a). Homogenous magnetic nanoparticles solutions, with different concentration 0, 5, 10, 20 and 50 mg/L, are adopted.

Besides, as the operating steps described above, 1 mL magnetic nanoparticle suspension (5 mg/L) with 10 μL MB is injected into the cuvette. A camera from the top view is used to record the radial distribution of MB at the bottom of cuvette as shown in Fig. 2(b).

2.2. Concentration-measuring experiment

UV–vis spectrophotometer (Agilent Cary-60) is used to measure the

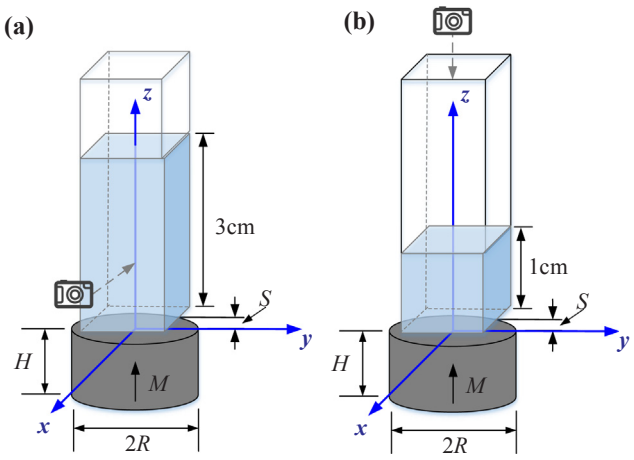

Fig. 2. The schematic diagram of dye-tracing experiment (a) front view, (b) top view.

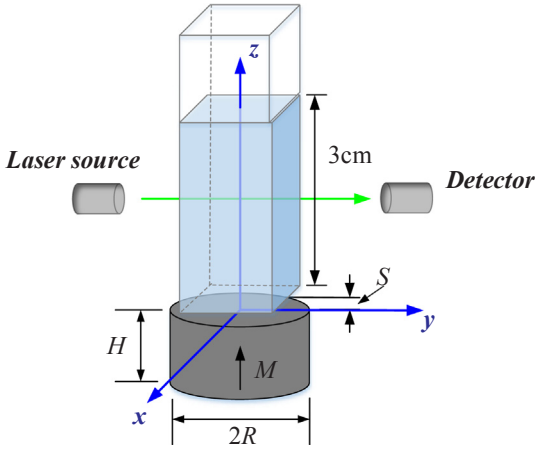

Fig. 3. The schematic diagram of concentration-measuring experiment.

absorbance of the MNPs solution. As shown in Fig. 3, the monochromatic light beam with wavelength of 530 nm is employed to measure the light absorbance of the MNPs solution at different location (z = 6 mm and z = 15 mm).

With the measured light absorbance, the particle concentration can be derived from the theory of Beer-Lambert law as given in Eq. (1) [21],

$$A = \varepsilon l \phi \tag{1}$$

where A is light absorbance, ε is the light absorptivity of MNPs, l is the optical path length, and ϕ is the concentration of particles. A normalized MNP concentration with respect to its initial concentration is adopted to analyze the spatial and temporal variation of ϕ after introducing external magnetic field, which is calculated as follows:

$$\phi_{N,MNP} = \frac{A - A_0}{A_i - A_0} \tag{2}$$

where A_0 is the light absorption of the distilled water and A_i is the initial light absorption of the MNPs solution.

3. Analytical method

3.1. Magnetic field

The equivalent current source (ECS) method, which is introduced by Furlani [22], is adopted to analyze the magnetic field of cylindrical permanent magnet. With respect to the principle of ECS method, a cylindrical permanent magnet can be reduced to an equivalent source term which is deduced from the magnetostatic field theory with the hypothesis that the magnetization of the magnet is constant [23].The schematic diagram of analytical model is shown in Fig. 4(a). Due to the axisymmetric characteristic of magnet, the r and z are used to describe the distribution of the magnetic field.

It should be noted that there is a concave surface at the interior bottom of a standard cuvette [20]. Therefore, this special geometric construction of the bottom of cuvette, which is labeled by yellow line in Fig. 4(a), is also considered in our numerical analysis. This concave surface is regarded as a part of sphere surface with R_c = 3.5 mm and h_{max} = 0.8 mm. An enlarged schematic of the vertical section of interior bottom of a cuvette is shown in Fig. 4(b). The d_b is the distance from a point in computational domain to the bottom of the cuvette.

According to the ECS method, the magnetic field ($\boldsymbol{H}$) can be given as Eq. (3), where $\boldsymbol{e}_r$ and $\boldsymbol{e}_z$ is the unit vector in radial and axial direction, respectively.

$$\boldsymbol{H} = H_r \boldsymbol{e}_r + H_z \boldsymbol{e}_z \tag{3}$$

H_r and H_z are the radial and axial component of the magnetic field strength, which are given as [24]

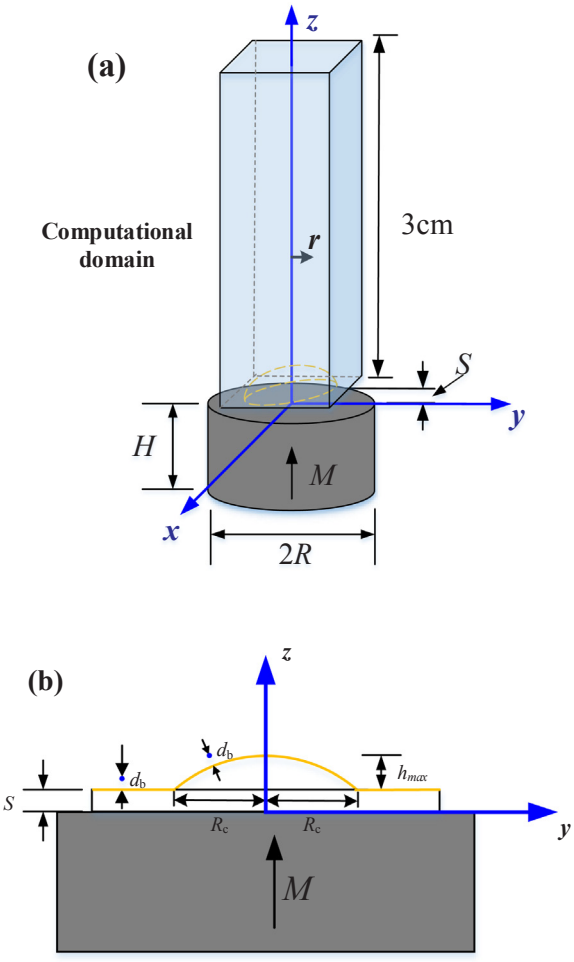

Fig. 4. The schematic diagram of analytical model (a), and the vertical section of interior bottom of a cuvette (b).

$$H_r = \frac{M}{2\pi} \times \int_{-L}^{0} \frac{z - z'}{r[(R+r)^2 + (z-z')^2]^{1/2}} \cdot \left[\frac{R^2 + r^2 + (z-z')^2}{(R-r)^2 + (z-z')^2} \cdot E(k) - K(k) \right] dz' \tag{4}$$

$$H_z = \frac{M}{2\pi} \times \int_{-L}^{0} \frac{1}{[(R+r)^2 + (z-z')^2]^{1/2}} \cdot \left[\frac{R^2 - r^2 - (z-z')^2}{(R-r)^2 + (z-z')^2} \cdot E(k) + K(k) \right] dz' \tag{5}$$

where K(k) and E(k) are the complete elliptic integrals of the first and second kind, respectively [12],

$$K(k) = \int_0^{\frac{\pi}{2}} \frac{1}{\sqrt{1 - k^2 \sin^2 \Phi}} d\Phi, \quad E(k) = \int_0^{\frac{\pi}{2}} \sqrt{1 - k^2 \sin^2 \Phi}\, d\Phi \tag{6}$$

where

$$k = \sqrt{\frac{4Rr}{(R+r)^2 + (z-z')^2}} \tag{7}$$

3.2. Kelvin force

The Kelvin force can be derived by regarding the MNP as equivalent magnetic point dipoles, as shown in Eq. (8) [25].

$$\boldsymbol{F}_m = \mu_f (\boldsymbol{m}_{p,eff} \cdot \nabla) \boldsymbol{H} \tag{8}$$

The μ_f is the permeability of carrier fluid, which is assumed to be

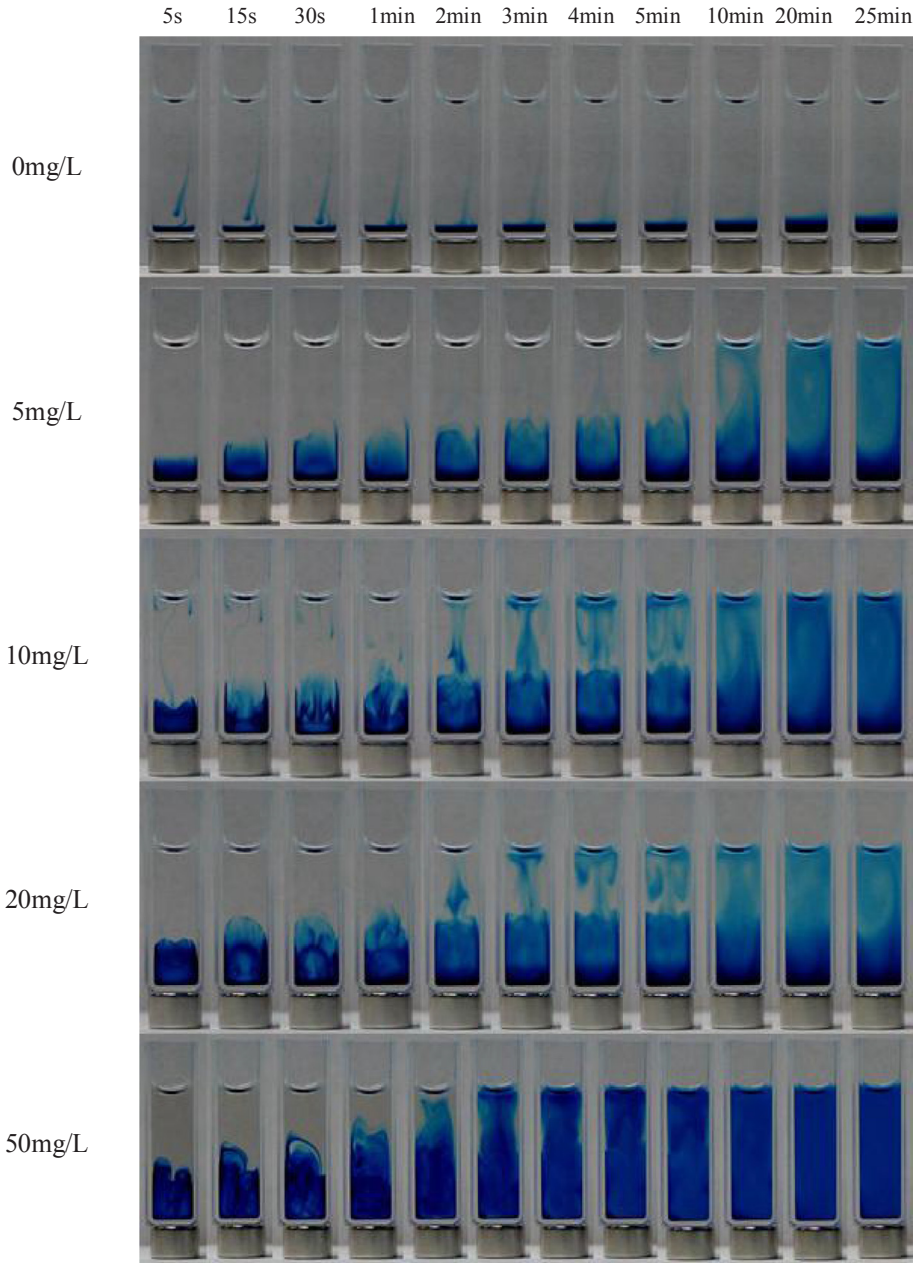

Fig. 5. The visualization forced convection of carrier fluid with different particle concentration (from 0 to 50 mg/L) for the first 25 min after being subjected to a cylindrical permanent magnet.

nonmagnetic ($\mu_f = \mu_0$). The effective moment can be given by taking the self-demagnetization field of particle into account [26].

$$\boldsymbol{m}_{p,eff} = V_p f(H)\boldsymbol{H} \tag{9}$$

where

$$f(H) = \begin{cases} \frac{3(\chi_p - \chi_f)}{(\chi_p - \chi_f)+3} & H < \left(\frac{(\chi_p - \chi_f)+3}{3\chi_p}\right)M_{sp} \\ M_{sp}/H & H \geqslant \left(\frac{(\chi_p - \chi_f)+3}{3\chi_p}\right)M_{sp} \end{cases} \tag{10}$$

and V_p is the volume of the particle and H is the strength of external magnetic field. In this equation, χ_p and χ_f are the magnetic susceptibilities of particle and fluid, respectively. The M_{sp} is the saturation magnetization of the particle. Considering the material of carrier fluid (water, $\chi_f = 0$), the Eq. (10) can be simplified as follows,

$$f(H) = \begin{cases} \frac{3\chi_p}{\chi_p + 3} & H < \left(\frac{\chi_p + 3}{3\chi_p}\right)M_{sp} \\ M_{sp}/H & H \geqslant \left(\frac{\chi_p + 3}{3\chi_p}\right)M_{sp} \end{cases} \tag{11}$$

4. Computational model

4.1. Uncoupled model

In the uncoupled model, the interaction between the particles and the carrier fluid is negligible. Besides, since the magnetic nanoparticles suspension with initial particle volume fraction $c_0 = 1 \times 10^{-6}$ is adopted, the interactions between the particles are ignored according to the theory of Furlani [1]. The drift-diffusion equation is adopted to investigate the influence of the Brownian motion on the distribution of particle volume fraction c as given in Eq. (12) [27].

$$\frac{\partial c}{\partial t} + \nabla\cdot(c\boldsymbol{v}_p) = \nabla\cdot(D\nabla c) \tag{12}$$

where $D = kT/(6\pi\eta R_p)$ is the diffusion coefficient, and the velocity of particle $\boldsymbol{v}_p$ is given by a balance between the fluidic viscous force and the magnetic force as shown in Eq. (13). The T (= 298 K) and η (= 0.001 $N{\cdot}sm^{-2}$) are the temperature and the viscous of the carrier fluid, respectively. The R_p is radius of the particles.

$$\boldsymbol{v}_p = \boldsymbol{F}_m/(6\pi\eta R_p) \tag{13}$$

4.2. Coupled model

In the uncoupled model, the carrier fluid is assumed to be stagnant and remains unaltered by the motion of the particles [14]. However, the particle migration would certainly induce the flowing of the carrier fluid, and the particle-induced fluid would alter the trajectory of the particle in turn. Therefore, a coupled model is adopted to describe the influence of the interaction between the particles and carrier fluid on the distribution of c. It is worth noting that the drift-diffusion Eq. (12) is still used to predict the behavior of particles, except that the particle velocity is given as

$$\boldsymbol{v}_p = \boldsymbol{u} + \boldsymbol{F}_m/(6\pi\eta R_p) \tag{14}$$

where $\boldsymbol{u}$ is the velocity of carrier fluid. The Navier-Strokes equation is adopted to describe the flow field of incompressible liquid.

$$\begin{aligned} \nabla\cdot\boldsymbol{u} &= 0 \\ \rho\left(\frac{\partial \boldsymbol{u}}{\partial t} + (\boldsymbol{u}\cdot\nabla)\boldsymbol{u}\right) &= -\nabla P + \eta\nabla^2\boldsymbol{u} + \boldsymbol{F}_{vol} \end{aligned} \tag{15}$$

where η is the dynamic viscosity of the fluid. The volume force $\boldsymbol{F}_{vol}$, which is induced by the external magnetic field, can be given as [14]

$$\begin{aligned} \boldsymbol{F}_{vol} &= n\boldsymbol{F}_m = n\mu_f V_p f(H)(\boldsymbol{H}\cdot\nabla)\boldsymbol{H} \\ &= c\mu_f f(H)(\boldsymbol{H}\cdot\nabla)\boldsymbol{H} \end{aligned} \tag{16}$$

where n is the number of particles in unit volume. By introducing the effect of the volume force, the drift-diffusion equation can be coupled with the flow field equation, in which the interaction between the particles and carrier fluid can be taken into account.

5. Results and discussions

5.1. Forced convection of carrier fluid

The dye-tracing method is adopted to observe the convective kinetics of fluid induced by magnetophoresis of MNP. As shown in Fig. 5, the flowing of fluid after the introduction of a cylindrical permanent magnet is recorded within 25 min for different particle concentration.

For the case with no MNP (0 mg/L), MB diffuses slowly in a limited time due to the thermal motion. As the particle concentration increases to 5 mg/L, the dye molecules move upward quickly, and the dye molecules at the top of solution go down inversely at 10 min, forming an obvious vortex. Furthermore, with the increase of particles concentration, this phenomenon occurs in a much shorter period of time, and more vortexes can be observed, for instance, two vortexes in 10 mg/L at 30 s. More specially, the duration that the dye molecules need to disperse in carrier fluid homogeneously decreases with the increase of particle concentration. This phenomenon implies that the magnetophoresis of MNP provides a means of accelerating mix of two different solutions.

Except for the axial movement of carrier fluid, its radial kinetics are also recorded as shown in Fig. 2(b), in which 1 mL MNP solution is used. In this case, only 5 mg/L MNP solution is adopted as shown in Fig. 6. This is because the rapid convection of dye molecules in high particle concentration gives rise to more dye molecules suspended at the top of solution in a short time, which results in difficulty in capturing the radial motion of carrier fluid with the limit of camera.

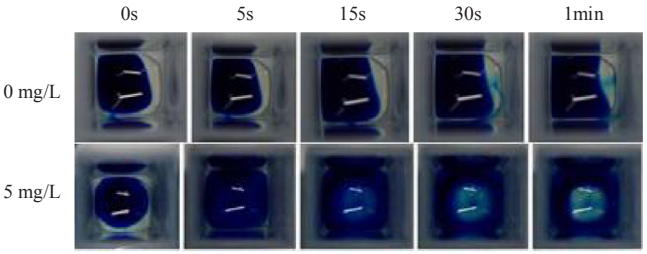

Fig. 6. The radial distribution of MB with different concentrations (0 and 5 mg/L) for the first 1 min after being subjected to a cylindrical permanent magnet.

As the particle concentration is 0 mg/L, slight diffusion of MB can be observed, which results from the Brownian motion of dye molecules. However, with the addition of magnetic nanoparticles (5 mg/L), most of MB molecules are pushed away from the center of the bottom of cuvette and tend to accumulate at the periphery of cuvette, forming a ring. The outward-radial motion and upward-axial convection of the carrier fluid should be induced by the magnetophoresis of MNP.

5.2. Magnetophoresis of MNP

The variation of particle concentration after the introduction of external cylindrical permanent magnet is recorded by using UV–vis spectrophotometer. As shown in Fig. 7, for the MNP solution with initial concentration of 5 mg/L, the variation of normalized particle concentration at z = 6 mm and z = 15 mm is presented. At z = 6 mm, the $\phi_{N,MNP}$ decreases rapidly over the time and reaches a stable value at about 400 s. It should be noted that, there is a difference in the concentration of MNPs at different positions in the cuvette. The MNP concentration decreases faster at z = 6 mm than at z = 15 mm.

At z = 15 mm, the variation of $\phi_{N,\ MNP}$ for different initial concentrations of MNP is shown in Fig. 8, from which we can derive that the falling velocity of particle concentration increases with the increase of initial concentration of MNP, implying an enhancing movement of MNP.

The axial distribution (r = 0) of axial magnetic force (F_{mz}) is shown in Fig. 9 for better understanding the movement of particles at different locations. The amplitude of F_{mz} decreases with the increase of the distance to permanent magnet. Furthermore, it shows that F_{mz} is close to zero with $z \geq 10$ mm. It means that the MNPs can be driven downward directly by the magnetic force in less than 10 mm from the magnet. The

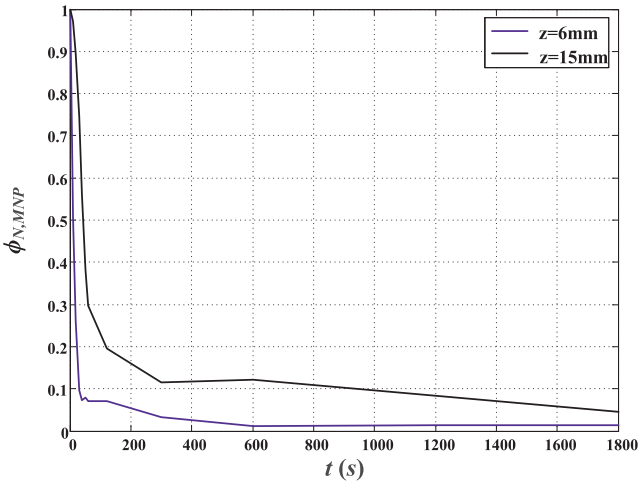

Fig. 7. The variation of normalized particle concentration $\phi_{N,\ MNP}$ at z = 6 mm and z = 15 mm with c_0 = 5 mg/L.

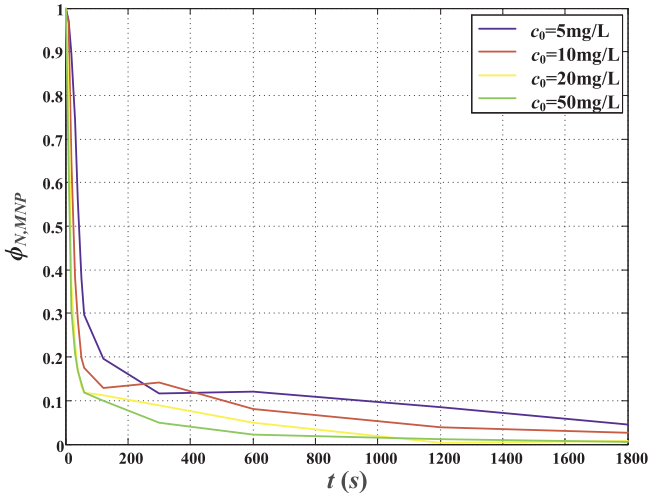

Fig. 8. The variation of normalized particle concentration $\phi_{N,\ MNP}$ at $z = 15$ mm with $c_0 = 5$ mg/L, 10 mg/L, 20 mg/L, 50 mg/L.

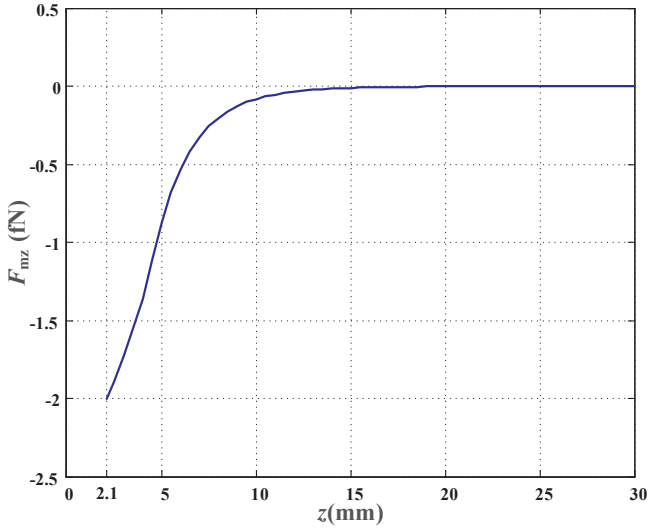

Fig. 9. The axial distribution of F_{mz} at $r = 0$.

movement of the MNPs out of this region should be governed by other factors. The flow of fluid (close to the magnet) induced by the magnetophoresis of MNPs as shown in the dye-tracing experiment should contribute to the motion of MNPs far from the magnet ($z \geq 10$ mm), which feel weak magnetic force.

In order to get insight into the intrinsic mechanism of magnetophoresis of MNP, theoretical analysis is proposed to investigate the influence of external magnetic field and particle-fluid interaction on the flowing of carrier fluid and the distribution of particle volume fraction. From the experimental results, we derive that the motion of particle and fluid close to the bottom of the cuvette is more intense than that away from the magnet, which is related to the powerful Kelvin force near the magnet. Then, the distribution of the axial and radial component of Kelvin force acting on magnetic nanoparticles with $\chi_p = 1.4$ and $\chi_f = 0$ at $z = 1.3$ mm, 1.7 mm, 2.1 mm and 2.5 mm is analyzed by using closed-form magnetic field analysis as shown in Fig. 10. Considering the length of diagonal line of cross section of cuvette (~1.414 cm), the range of r is varying from 0 to 6 mm ($=R$).

One of the most interesting features of $|F_{mz}|$ at $z = 1.3$ mm is that it firstly increases with the increase of r, reaching the peak at $r = 5.5$ mm, and then decreases with the further increasing of r. Furthermore, the r corresponding to the maximum of $|F_{mz}|$ decreases with the increase of z. The negative F_{mz} drive MNP downward towards the bottom of the cuvette, which is the intrinsic mechanism of subsidence phenomenon of Figs. 7 and 8. From Fig. 10(b), we can derive that the $|F_{mr}|$ increases with the increase of r and obtains maximum at the margin of the magnet. Furthermore, the peak value of $|F_{mr}|$ decreases with the increase of z. Besides, a comparison of $|F_{mz}|$ and $|F_{mr}|$ denotes that $|F_{mz}|$ is always larger than $|F_{mr}|$ at the computational region, implying a faster sedimentation than a tendency of centering. With the combination of F_{mr} and F_{mz}, most of MNPs tend to accumulate at the region where their final location r_f is slightly smaller than their initial location r_0.

With the closed-form analysis of Kelvin force, the uncoupled model is adopted to investigate the three-dimensional distribution of the particles concentration in the presence of a cylindrical permanent magnet. The distribution of the particle concentration at y-z plane ($z \leq 6$ mm) with initial particle volume fraction $c_0 = 1 \times 10^{-6}$ ($\phi = 5$ mg/L) at 10 s and 20 s is shown in Fig. 11. The distribution of c at the region above $z = 6$ mm presents a similar profile as compared with that at the region 3 mm $< z <$ 6 mm as $t \leq 20$ s.

At $t = 10$ s, the c decreases with the increase of distance d_b as $d_b < 0.5$ mm, above where the particles stably suspend in the carrier fluid and little variation of c is observed. However, at $t = 20$ s, the c decreases with the increase of d_b as $d_b < 0.8$ mm. This phenomenon

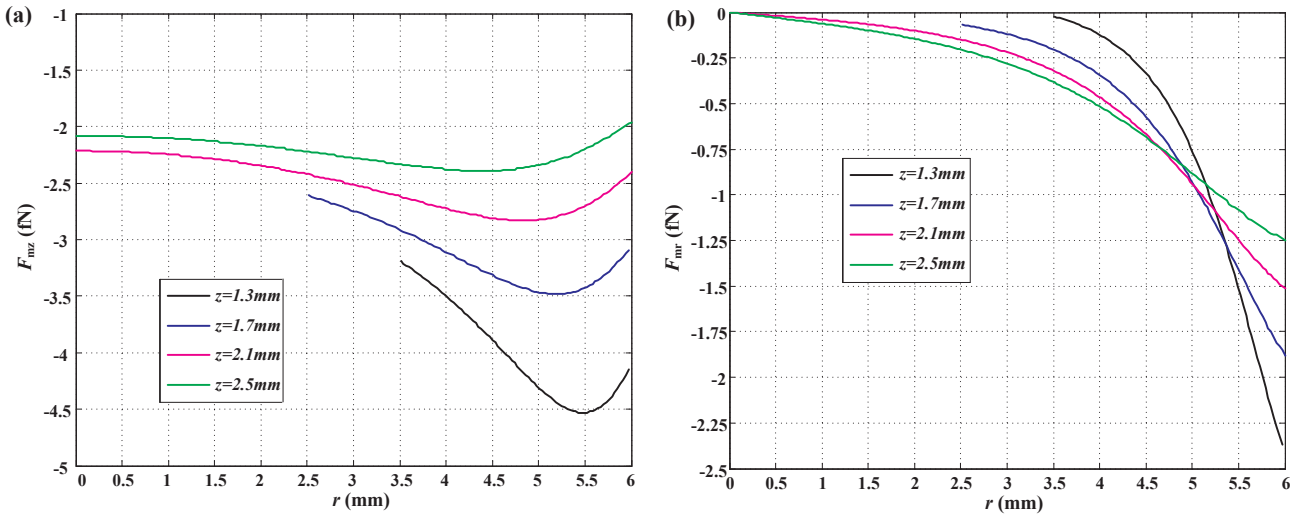

Fig. 10. The distribution of F_{mz} (a) and F_{mr} (b) at $z = 1.3$ mm, 1.7 mm, 2.1 mm and 2.5 mm.

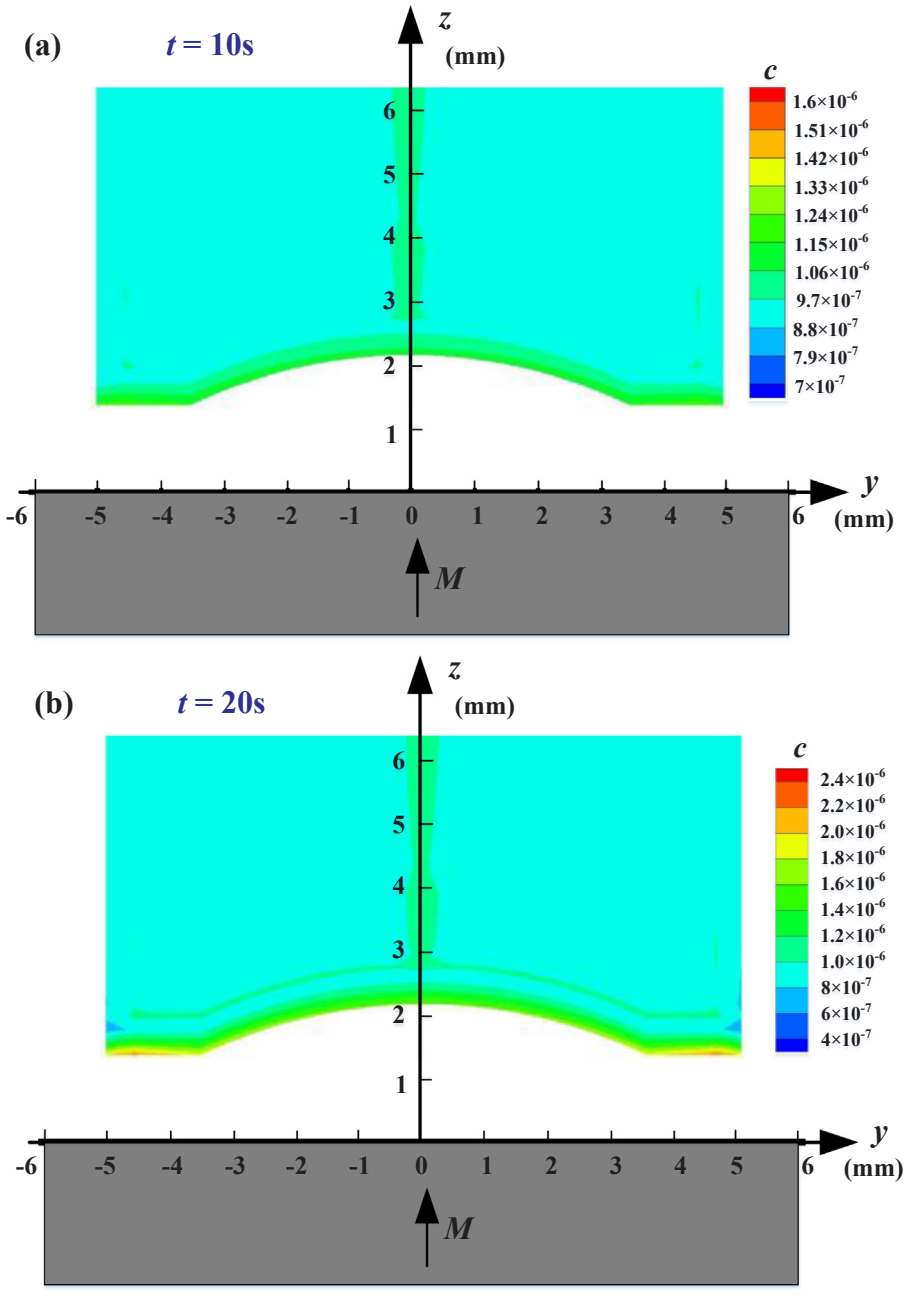

Fig. 11. The distribution of c at z-y plane ($z \leq 6$ mm) at $t = 10$ s (a) and $t = 20$ s (b) by using uncoupled model with $c_0 = 1 \times 10^{-6}$.

results from the rapid subsidence of particles that close to the magnet and the accumulation of attracted particles. Besides, there is a local region with high particle concentration at $d_b \sim 0.8$ mm, which results from the sedimentation of particles from upper fluid. Furthermore, as time goes on, more and more particles are captured at the bottom of cuvette. More specially, as $z > 3$ mm, an obvious high particle concentration around the axis of cuvette is formed, which should be related to the centripetal F_{mr}. Besides, the distribution of c at the bottom of cuvette shows relatively distinct variation as compared with the initial concentration c_0 as shown in Fig. 12.

At $t = 10$ s, most of the particles separated from the carrier fluid tend to accumulate towards the margin of the magnet. As time goes on, an apparent annular morphology is formed under the action of F_{mr} and F_{mz}, showing maximum near the locations $r = 4$ mm as shown in Fig. 12(b). Besides, it should be noted that the asymmetric profile of c near the boundary should be result from the geometry of a cube-shaped cuvette.

According to the research of Leong [19], the interaction between the particles and the surrounding fluid plays an essential role in controlling the particle motion and the flow field. Then, by introducing the momentum transfer between these two species, the coupled model is adopted to describe the magnetophoresis of magnetic nanoparticles. In order to present the distribution of c more clearly, an average of particles volume fraction c_{ave} at a given r is proposed as defined in Eq. (17)

$$c_{ave} = \frac{\sum_{i=1}^{N(r)} c(x, y, z)}{N(r)} \tag{17}$$

where $N(r)$ is the number of cells whose distance to z axis is r.

As shown in Fig. 13(a), an annular profile with four obvious regions of high particle volume fraction is formed at the bottom of cuvette when $t = 10$ s. The distribution of c_{ave} in Fig. 13(b), in which the orange color presents concave surface, denotes that most of the captured

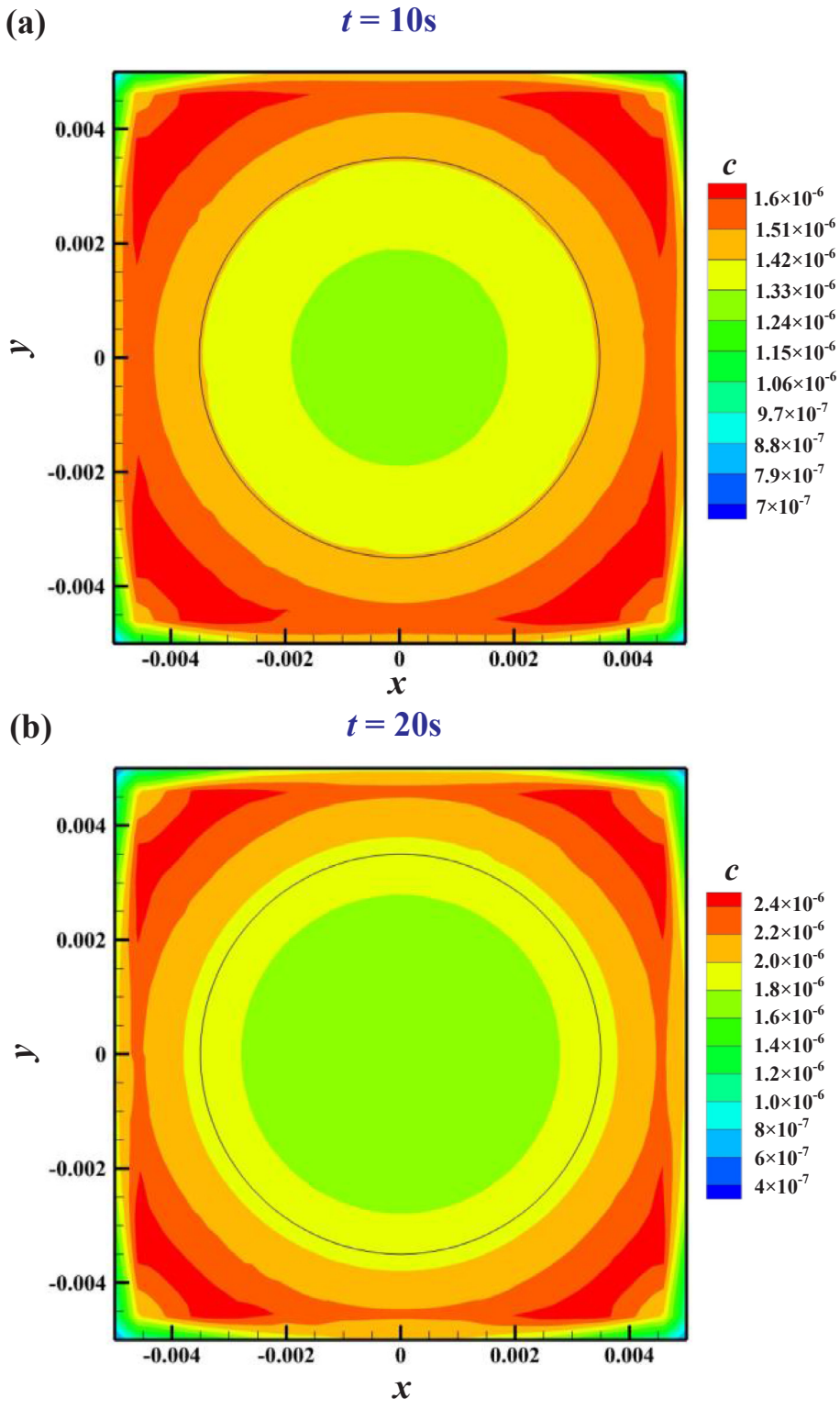

Fig. 12. The distribution of c at the bottom of cuvette when $t = 10$ s (a) and $t = 20$ s (b) by using uncoupled model with $c_0 = 1 \times 10^{-6}$.

particles tend to accumulate at the region near $r = 0.7R$. Besides, a comparison of c_{ave} between the uncoupled model and coupled mode implies that the r corresponding to a maximum of c_{ave} moves toward center under the effect of particle-fluid interaction, which also speeds up the accumulation of particles. This also implies that the interaction between the particles and carrier fluid not only plays a significant role in influencing the behavior of the magnetic nanoparticles, but also gradually dominates the kinetics of carrier fluid, which can be observed from the distribution of velocity and streamline as shown in Fig. 14.

From Fig. 14, we can observed that the v_y shows dramatic variation as $z < 4$ mm, whereas v_z presents distinct variation in all computational domain. Furthermore, due to the effect of magnetophoresis of MNPs, two vortexes are formed near the bottom of the cuvette, pushing the particles moving towards the margin of concave surface. Besides, another two vortexes in $z > 8$ mm drive nanoparticles suspending in upper fluid downward towards the magnet.

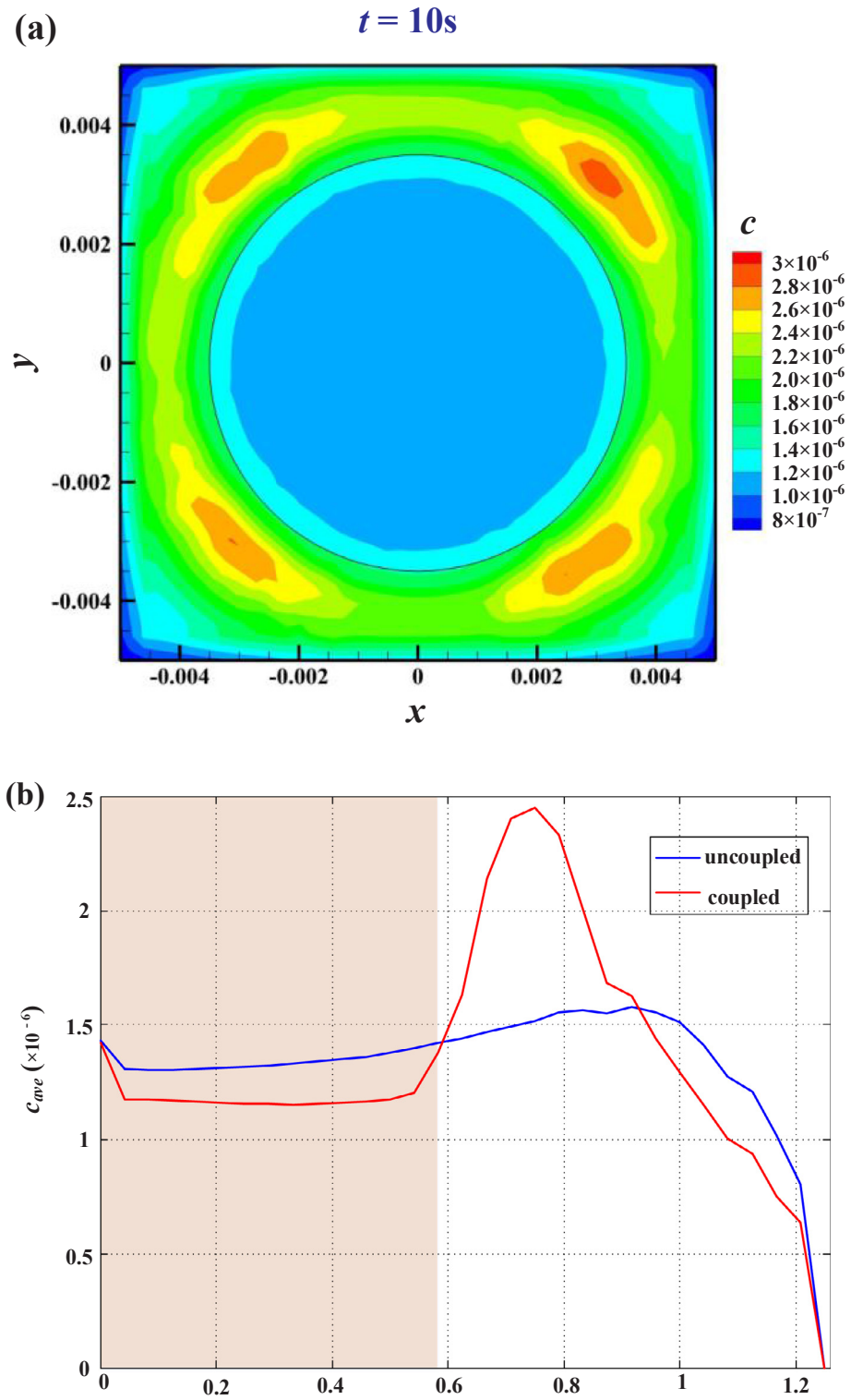

Fig. 13. The distribution of c (a) and c_{ave} (b) at the bottom of cuvette when $t = 10$ s by using coupled model with $c_0 = 1 \times 10^{-6}$.

As time goes on, an obvious variation of c and kinetic of carrier fluid can be observed as shown in Figs. 15 and 16.

Unlike the distribution of c in Fig. 13, the region with high c shows a tendency to concentrate toward the center at $t = 13$ s as shown in Fig. 15(a). Furthermore, an expansion of the regions with high c can be observed. Besides, a comparison of c_{ave} at $t = 10$ s and $t = 13$ s indicates that the number of particles that deposit at the concave surface increases over time and most of particles tend to accumulate at the margin of concave surface when $t = 13$ s, which should be due to the accumulation of particles from upper fluids. The distributions of fluid velocity in y-z plane at $t = 13$ s are shown in Fig. 16.

As compared with that of Fig. 14, the maximum of $|v_y|$ and $|v_z|$ increases over time. Furthermore, the fluid near the bottom of cuvette shows opposite flowing direction, flowing from the boundary of cuvette to the center. This is precisely why more and more particles tend to accumulate at the concave surface.

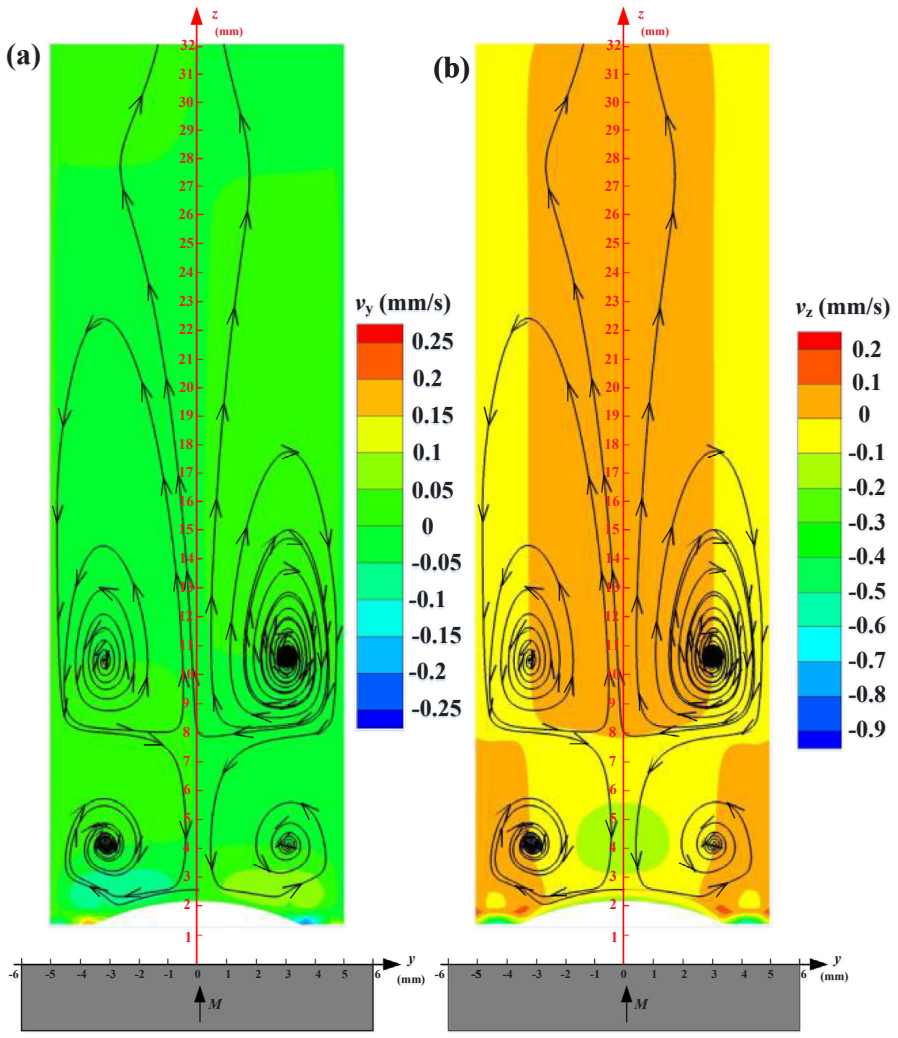

Fig. 14. The distribution of v_y (a), v_z (b) and streamline (black line) at $t = 10$ s by using coupled model with $c_0 = 1 \times 10^{-6}$.

Finally, it should be noted that the evolution of MNPs concentration shown in Figs. 7 and 8 is different from that reported in [19]. In [19], in thousands of minutes, the normalized separation kinetic profiles of the MNPs solution almost collapsed into a single curve, regardless of the different initial particle concentration or different measurement location. In present work, the faster and more variant sedimentation in Figs. 7 and 8 should be closely related with the particle-to-particle interaction. Therefore, it is not appropriate to only use the initial concentration of particles to predict the effect of interactions between particles. According to the theory of Faraudo, the aggregation parameter is proposed to predict the effect of particle-to-particle interaction as defined in Eq. (18) [28]:

$$N^* = \sqrt{c_0 e^{\Gamma - 1}} \tag{18}$$

where c_0 is the initial volume fraction of particles in the solution and Γ is magnetic coupling parameter. With present experimental configurations, N^* is larger than unity even at the lowest MNP concentration of 5 mg/L. It implies that the particle-to-particle interaction also plays a significant role in affecting the magnetophoresis of MNPs, whereas this is not considered in our present analytical model.

6. Conclusion

The hydrodynamics of carrier fluid and magnetophoresis of MNP, suspending in water, in the presence of a cylindrical permanent magnet are analyzed by using experimental and numerical method. With the introduction of magnetic field, a forced convection of carrier fluid is recorded by using dye-tracing method, in which the MB molecules can visualize the flowing of carrier fluid induced by the magnetophoresis of MNPs. Moreover, higher concentration of MNPs results in more violent flow of the fluid, even the occurrence of vortex-like flow. Besides, with the effect of magnetophoresis of MNPs, most of fluid are pushed towards the direction away from the center at the bottom of the cuvette. These experiments denote that the particle-fluid interaction and magnetophoresis of MNP play an important role in affecting the kinetics of carrier fluid.

Besides, the magnetophoresis of the magnetic nanoparticles is also analyzed by using concentration-measuring experiments and a coupled particle-fluid model. The concentration-measuring experiments show that the MNP concentration close to the permanent magnet decreases faster than that far away from it. Higher initial concentration of MNPs leads to more obvious variation of MNP concentration. In order to get insight into the physic mechanism of magnetophoresis, the coupled model is also adopted to investigate the variation of particle concentration and streamline of carrier fluid. Furthermore, as a comparison, an uncoupled model, in which the carrier fluid is assumed stagnant and remains unaltered by the motion of the particles, is also adopted to analyze the magnetophoresis of MNP. An annulus with four regions of high particle volume fraction is formed around the margin of concave surface in coupled model. Furthermore, this annulus tends to

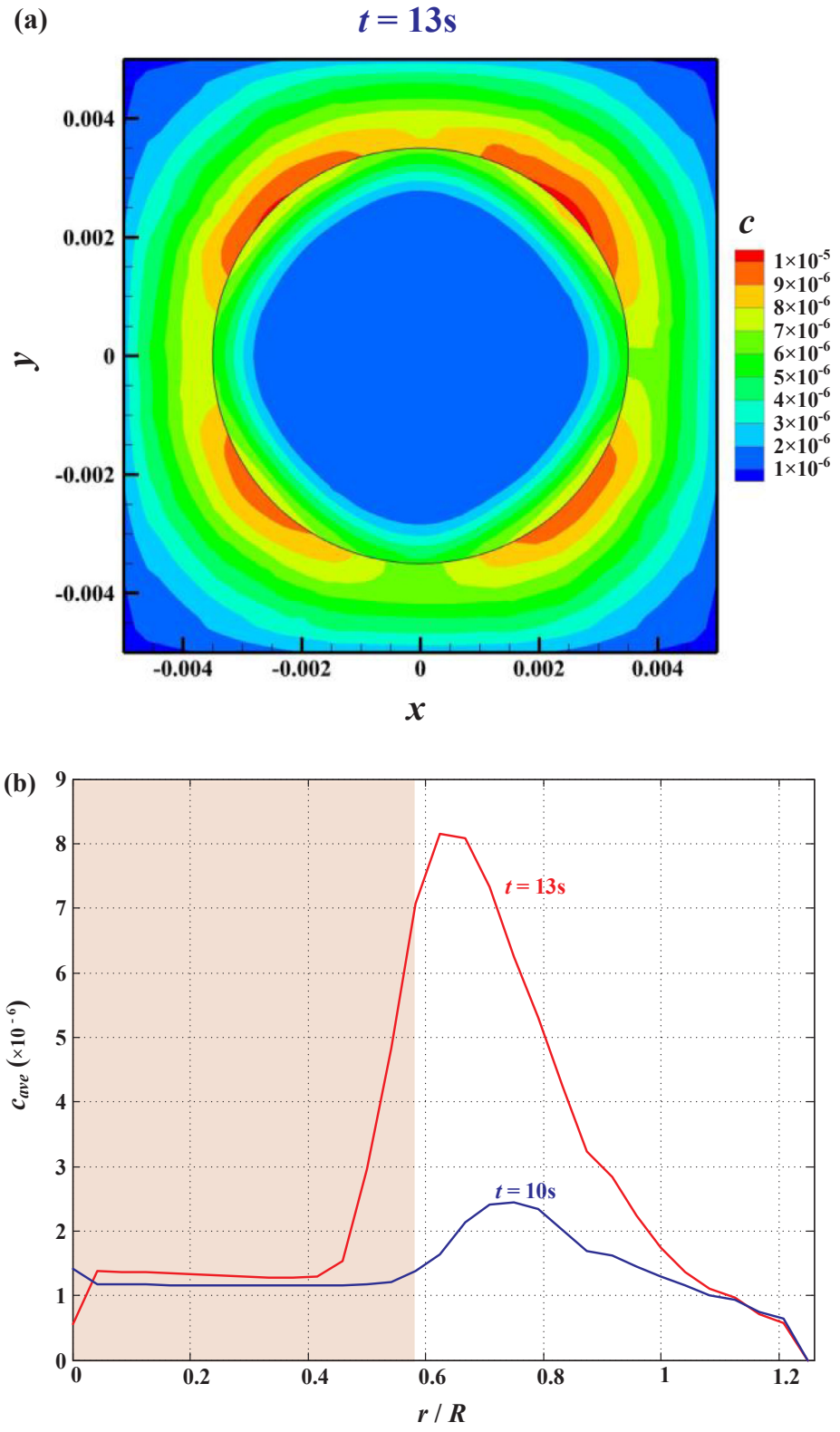

Fig. 15. The distribution of c (a) and cave (b) at the bottom of cuvette when t = 13 s by using coupled model with $c_0 = 1 \times 10^{-6}$.

move toward center as time goes on, which is different to the ring moving toward margin of the magnet in the uncoupled model. Besides, the distribution of velocity of fluid illustrates the flowing of carrier fluid and particle-induced vortexes. This phenomenon is consistent with the formation of vortexes in dye-tracing experiments.

The comparison between experimental and numerical results indicates that the interaction between particles also plays an important role in enhancing the sedimentation of particles.

Acknowledgements

The work was supported by the National Natural Science

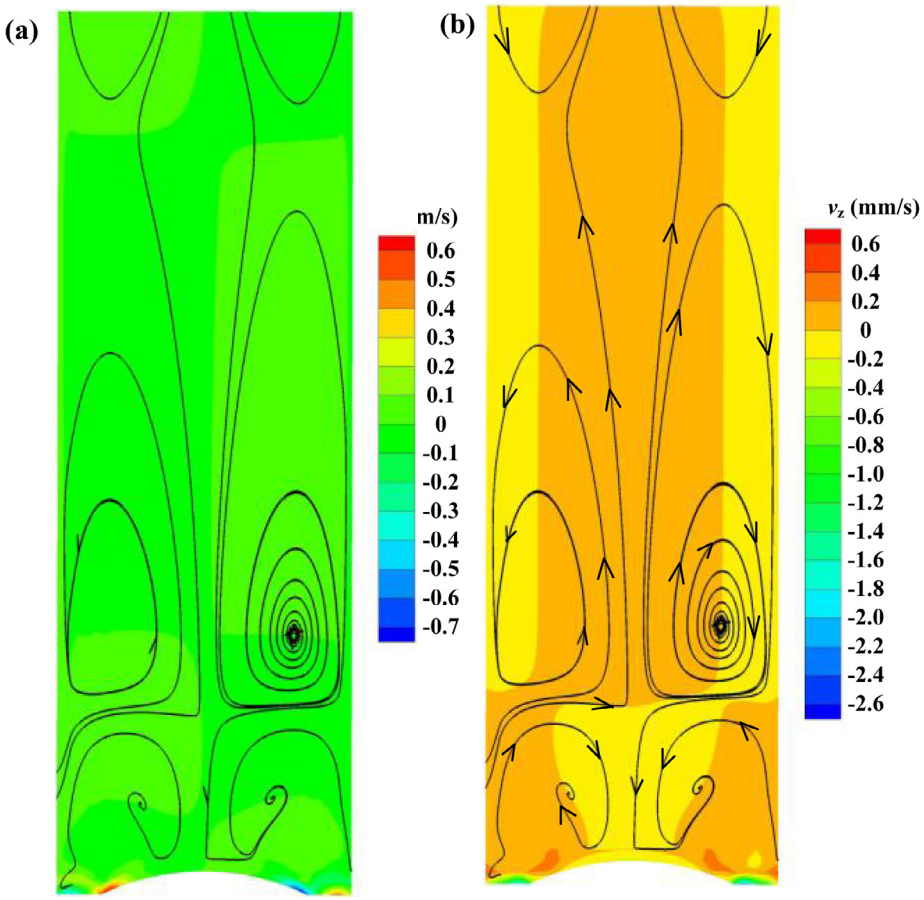

Fig. 16. The distribution of v_y (a) and v_z (b) in *y*-*z* plane at $t = 13$ s by using coupled model with $c_0 = 1 \times 10^{-6}$, and the black lines show the distribution of streamline.

Foundation of China under project 51777148.

References

[1] E.P. Furlani, Magnetic biotransport: analysis and applications, Materials 3 (2010) 2412–2446.
[2] R. Ganguly, A.P. Gaind, S. Sen, I.K. Puri, Analyzing ferrofluid transport for magnetic drug targeting, J. Magn. Magn. Mater. 289 (2005) 331–334.
[3] A. Fouriki, N. Farrow, M.A. Clements, J. Dobson, Evaluation of the magnetic field requirements for nanomagnetic gene transfection, Nano Rev. 1 (2010).
[4] A.L. Gassner, M. Abonnenc, H.X. Chen, J. Morandini, J. Josserand, J.S. Rossier, J.M. Busnel, H.H. Girault, Magnetic forces produced by rectangular permanent magnets in static microsystems, Lab Chip 9 (2009) 2356–2363.
[5] S.C. McBain, U. Griesenbach, S. Xenariou, A. Keramane, C.D. Batich, E.W. Alton, J. Dobson, Magnetic nanoparticles as gene delivery agents: enhanced transfection in the presence of oscillating magnet arrays, Nanotechnology 19 (2008) 405102.
[6] C. Huang, K.G. Neoh, L. Wang, E.-T. Kang, B. Shuter, Magnetic nanoparticles for magnetic resonance imaging: modulation of macrophage uptake by controlled PEGylation of the surface coating, J. Mater. Chem. 20 (2010) 8512.
[7] C. Sun, J.S. Lee, M. Zhang, Magnetic nanoparticles in MR imaging and drug delivery, Adv. Drug Delivery Rev. 60 (2008) 1252–1265.
[8] M. Bahiraei, M. Hangi, Flow and heat transfer characteristics of magnetic nanofluids: A review, J. Magn. Magn. Mater. 374 (2015) 125–138.
[9] N. Modak, A. Datta, R. Ganguly, Numerical analysis of transport and binding of a target analyte and functionalized magnetic microspheres in a microfluidic immunoassay, J. Phys. D: Appl. Phys. 43 (2010) 485002.
[10] X. Xue, E.P. Furlani, Template-assisted nano-patterning of magnetic core-shell particles in gradient fields, Phys. Chem. Chem. Phys. 16 (2014) 13306–13317.
[11] Z. Shi, J. Sun, S. Jia, P. Zhang, Simulation of magnetophoresis of magnetic nanoparticles in liquids, J. Phys. D: Appl. Phys. 49 (2016) 335005.
[12] E.P. Furlani, Y. Sahoo, K.C. Ng, J.C. Wortman, T.E. Monk, A model for predicting magnetic particle capture in a microfluidic bioseparator, Biomed. Microdevices 9 (2007) 451–463.
[13] R. Gerber, M. Takayasu, F. Friedlaender, Generalization of HGMS theory: The capture of ultra-fine particles, Shock 19 (1983) 2115–2117.
[14] Q. Cao, X. Han, L. Li, Numerical analysis of magnetic nanoparticle transport in microfluidic systems under the influence of permanent magnets, J. Phys. D: Appl. Phys. 45 (2012) 465001.
[15] S.A. Khashan, E.P. Furlani, Coupled particle-fluid transport and magnetic separation in microfluidic systems with passive magnetic functionality, J. Phys. D: Appl. Phys. 46 (2013) 125002.
[16] B. Teste, F. Malloggi, A.L. Gassner, T. Georgelin, J.M. Siaugue, A. Varenne, H. Girault, S. Descroix, Magnetic core shell nanoparticles trapping in a microdevice generating high magnetic gradient, Lab Chip 11 (2011) 833–840.
[17] V. Schaller, U. Kräling, C. Rusu, K. Petersson, J. Wipenmyr, A. Krozer, G. Wahnström, A. Sanz-Velasco, P. Enoksson, C. Johansson, Motion of nanometer sized magnetic particles in a magnetic field gradient, J. Appl. Phys. 104 (2008).
[18] O. Mykhaylyk, D. Lerche, D. Vlaskou, V. Schoemig, T. Detloff, D. Krause, M. Wolff, T. Joas, S. Berensmeier, C. Plank, Magnetophoretic velocity determined by space- and time-resolved extinction profiles, IEEE Magn. Lett. 6 (2015) 1–4.
[19] S.S. Leong, Z. Ahmad, J. Lim, Magnetophoresis of superparamagnetic nanoparticles at low field gradient: hydrodynamic effect, Soft Matter 11 (2015) 7696 7696.
[20] S.S. Leong, Z. Ahmad, J. Camacho, J. Faraudo, J. Lim, Kinetics of low field gradient magnetophoresis in the presence of magnetically induced convection, J. Phys. Chem. C 121 (2017) 5389–5407.
[21] M.A. Lema, E.M. Aljinovic, M.E. Lozano, Using a homemade spectrophotometer in teaching biosciences, Biochem. Mol. Biol. Educ. 30 (2010) 106–110.
[22] E.P. Furlani, Permanent Magnet and Electromechanical Devices: Materials, Analysis, and Applications, Academic Press, 2001.
[23] J. Sun, Z. Shi, J. Bai, S. Jia, P. Zhang, Numerical investigation on the magnetic field of cylindrical permanent magnet for magnetic nanoparticles application, Nanotechnology (IEEE-NANO), 2015 IEEE 15th International Conference on, 2015, pp. 1041–1044.
[24] E.P. Furlani, X. Xue, Field, force and transport analysis for magnetic particle-based gene delivery, Microfluid. Nanofluid. 13 (2012) 589–602.
[25] E.P. Furlani, K.C. Ng, Nanoscale magnetic biotransport with application to magnetofection, Phys. Rev. E 77 (2008).
[26] S.A. Khashan, A. Alazzam, E.P. Furlani, Computational analysis of enhanced magnetic bioseparation in microfluidic systems with flow-invasive magnetic elements, Sci. Rep. 4 (2014) 5299.
[27] E.P. Furlani, K.C. Ng, Analytical model of magnetic nanoparticle transport and capture in the microvasculature, Phys. Rev.. E, Stat., Nonlinear, Soft Matter Phys. 73 (2006) 061919.
[28] J.S. Andreu, P. Barbero, J. Camacho, J. Faraudo, Simulation of magnetophoretic separation processes in dispersions of superparamagnetic nanoparticles in the noncooperative regime, J. Nanomater. 2012 (2012) 1–10.